Lab on a Chip

A connected cytoskeleton network generates axonal tension in embryonic drosophila

Journal:	*Lab on a Chip*
Manuscript ID	LC-ART-03-2019-000243.R1
Article Type:	Paper
Date Submitted by the Author:	12-Jul-2019
Complete List of Authors:	Fan, Anthony; University of Illinois at Urbana-Champaign Department of Mechanical Science and Engineering, JOY, MD SADDAM HOSSAIN; University of Illinois at Urbana-Champaign Saif, Taher; University of Illinois at Urbana-Champaign, Mechanical Science and Engineering

A connected cytoskeleton network generates axonal tension in embryonic *Drosophila*

Anthony Fan*[1], Saddam Joy[1], and Taher Saif†[1]

[1] *Department of Mechanical Science and Engineering, University of Illinois at Urbana-Champaign, Urbana, IL, USA*

August 14, 2019

Abstract

Axons of neurons are contractile, i.e., they actively maintain a rest tension. However, the spatial origin of this contractility along the axon, and the role of cytoskeleton in generating tension and sustaining rigidity are unknown. Here, using a microfluidic platform, we exposed a small segment of the axons of embryonic *Drosophila* motor neurons to specific cytoskeletal disruption drugs. We observed that a local acto-myosin disruption led to a total loss in axonal tension, with the stiffness of the axon remaining unchanged. A local disruption of microtubules led to a local reduction in bending stiffness, while tension remained unchanged. These observations demonstrated that contractile forces are generated and transferred along the entire length of the axon in a series fashion. Thus, a local force disruption results in a collapse of tension of the entire axon. This mechanism potentially provides a pathway for rapid tension regulation to facilitate physiological processes that are influenced by axonal tension.

Introduction

Mechanical tension has been shown to play an influential role in vesicle clustering[1], vesicle dynamics[2], neural excitability[3], axon growth[4,5], and genetic regulation[6]. Studies using glass needles[7,8], force probe[9], and fluidic flow[10] show that there exists a finite intrinsic tension in *in vitro* and *in vivo* neurons. Further evidence shows that mammalian brains also maintain a residual tension[11], which was speculated to drive cortical folding among other processes[12,13]. It is thus possible that a neuron can regulate its function by regulating its intrinsic tension.

How a neuron regulates its tension therefore warrants investigation. Several studies have shown that actin and myosin are responsible for generating tension, while microtubules act against tension[14–16]. Recently, it is further revealed that axonal tension has a coupled circumferential component, pointing to the hypothesis that tension is generated by a contractile network unaligned with the axis of the axon[17]. Super-resolution microscopy reveals that F-actin forms periodic rings along the length of the axon, with connecting spectrin tetramer in between each ring[18,19]. Myosin motors have also been shown to associate with the F-actin rings[20]. We therefore hypothesize that the contractile network works in series and tension is transmitted along the acto-myosin network of the axon.

Here, we test this hypothesis by disrupting a segment of axonal cytoskeletal proteins by partial chemical treatment—if the contractile network is indeed in series, a local disruption will lead to a total loss of tension. We achieved this by using a microfluidic device that can combine partial treatment with tension measurement[21]. We modeled the axon as a slender string subjected to a shear load. Flow rate was increased in a step-wise fashion to probe the elastic response of the axon. A global/partial chemical treatment could also be simultaneously applied. Such laminar flow allowed us to evaluate the stiffness and rest tension of axons under partial/global F-actin, myosin, and microtubules disruption.

*corresponding author: yungfan2@illinois.edu
†corresponding author: saif@illinois.edu

Materials & Methods

Drosophila culture

Drosophila culture followed standard procedure[22]. The fly line expressing green fluorescence protein (GFP) on neuronal membranes (5146) was purchased from Bloomington stock center (Bloomington, IN). Flies were placed in a culture chamber and embryos were collected on a grape-agar gel. Embryos of stage 16 were selected based on morphology.

Microfluidics setup

Sample preparation followed an established protocol[21]. Briefly, a dissected embryo was placed on a cover slip (12-545H; Fisher Scientific, Hampton, NH). A slab of patterned liquid silicon rubber (Bluestar LSR-4305) is positioned on top of the embryo and mounted directly to the cover slip. A suction flow is used to backfill the device to remove the bubbles trapped during assembly. Three other forward flows provide the saline side flows and the center flow containing the chemical treatment. The ratio of the volumetric flow rate of the 3 forward channels dictates the size and position of the center flow, allowing localized placement of the treatment. The total flow rate governs the shear load applied onto the axon (see mechanics model below).

Chemical treatment

Cytochalasin D (50 μg/mL), Nocodazole (15 μg/mL), Y-27632 (110 μM) were applied to the center flow to either partially or globally inhibit the respective proteins. Cytochalasin D and nocodazole were purchased from Sigma-Aldrich (St. Louis, MO) and Y-27632 from Cayman Chemical (Ann Arbor, MI).

Imaging

An inverted microscope (IX81; Olympus, Center Valley, PA) with standard GFP and mCherry filters was used. All images were acquired using a 20x/0.4 lens (LCPlanFI; Olympus, Center Valley, PA). Exposure time for axon imaging is set to 300ms. Red fluorescent beads of 0.1 μm in diameter (F8801; Thermo Fisher Scientific, Waltham, MA) were placed at the bottom of the glass slide (exposed to air). The best focal planes of the beads and the axon were identified. The distance d between the 2 planes minus the thickness t of the glass slide provided the elevation, z_a, of the axon from the glass surface (Fig. 1a).

Mechanics Model

The elevation of the axon, z_a, from the floor is used to estimate flow velocity and shear load. Our device can be approximated as a parallel plate setup (Fig. 1b) since the width w (1.5 mm) is much larger than the height h (0.2 mm). Given the no-slip boundary condition at the fluid-solid interface and the laminar flow condition at low Reynold's number, the flow profile is:

$$V(z) = V_{max}(1 - 4\frac{z^2}{h^2}) \tag{1}$$

where z is the direction perpendicular to the top and bottom surface, and z=0 is the mid-plane of the chamber. The constant V_{max} could be determined by integrating $V(z)$ over z multiplied by the width, and matching the applied volumetric flow rate, Q_{app}, from the syringe pump:

$$Q_{app} = w\int_{-\frac{h}{2}}^{\frac{h}{2}} V(z)dz = V_{max}w\int_{-\frac{h}{2}}^{\frac{h}{2}}(1 - 4\frac{z^2}{h^2})dz \tag{2}$$

As a result, the flow velocity felt by the axon is:

$$V(z_a) = \frac{Q_{app}}{w\int_{-\frac{h}{2}}^{\frac{h}{2}}(1 - 4\frac{z^2}{h^2})dz}(1 - 4\frac{{z_a}^2}{h^2}) \tag{3}$$

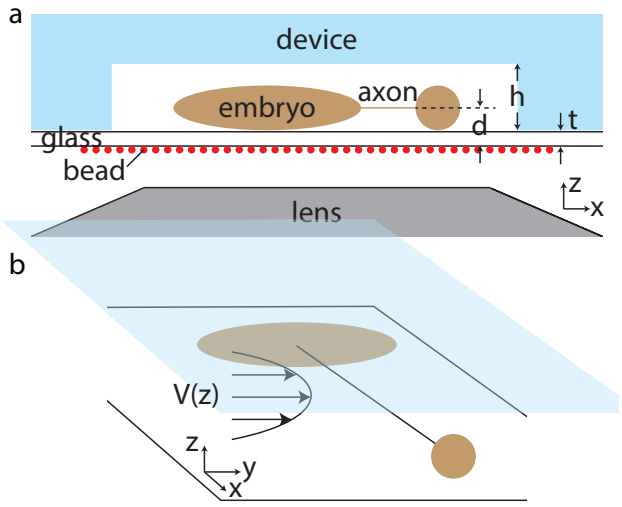

Figure 1: Schematics of the device. (a) A side-view of the device illustrating the position of the red fluorescence beads and their role in determining the elevation of the exposed axon, $z_a = d - t$. (b) The elevation of the exposed axon is important in determining the flow rate at that z-plane, which governs the shear load on the axon.

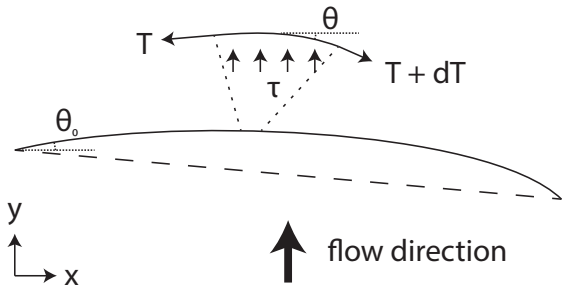

Figure 2: Free body diagram of the axon under a distributed load τ induced by the fluid flow.

The flow velocity can then be further converted to a shear load, given by $\tau = \frac{4\pi\mu V}{ln(\frac{3.7\nu}{rV})}$ [23], where μ is the dynamic viscosity, ν is the kinematic viscosity, and r is the radius of the axon.

The shear load would lead to a force balance (Fig. 2) in the form of:

$$dT_x = 0 \tag{4}$$

$$dT_y = \tau dx \tag{5}$$

Eq. 4 & 5 can be rewritten as:

$$T_0\, cos\theta_0 = T\, cos\theta \tag{6}$$

$$d(T\, sin\theta) = \tau dx \tag{7}$$

where T_0 and θ_0 indicate tension and angle at the origin. Eq. 7 can then be reformulated to:

$$d(T_0\, cos\theta_0 \frac{dy}{dx}) = \tau dx \tag{8}$$

By performing integrations and applying the appropriate boundary conditions: 1) $y(x = 0) = 0$, and 2) $\frac{dy}{dx}\big|_{x=0} = tan\theta_0$, we arrived at the following expression for the profile of the axon subjected to a shear load of τ:

$$y = \underbrace{\frac{\tau}{2T_0\, cos\theta_0}}_{A(t)}\, x^2 + \underbrace{\tan\theta_0}_{B(t)}\, x \tag{9}$$

The profile of the axon was obtained from image analysis. The identified points along the axon were expressed as x-y coordinates. The points were then fit to Eq. 9 to obtain the constants A and B for each t with the point closest to the central nervous system (CNS) as the origin. By substituting Eq. 6 to Eq. 9, tension can also be expressed as:

$$T(x,t) = \frac{\tau}{2A(t)cos\theta(x,t)} \tag{10}$$

$$\overline{T}(t) = \frac{\int T(x,t)dx}{\int dx} = \frac{\tau}{2A(t)}\frac{\int sec\theta(x,t)dx}{\int dx} \tag{11}$$

$$= \frac{\tau}{2A(t)}\frac{\int ds(t)}{\int dx} \tag{12}$$

where $\overline{T}$ is the average tension along the axon, $\int ds$ is the arc length of the axon, and $\int dx$ is the projected length of the axon perpendicular to the flow direction. The arc length can be evaluated by using Eq. 9. The difference in arc lengths over time will also provide the stretch of the axon due to flow. The projected length does not vary significantly with time because it is perpendicular to the flow direction and thus can be prescribed based on the images.

Image Analysis

The following procedures were performed by a custom code written in MATLAB (Fig. S1). Image intensity profile along the y-axis for every x was collected and smoothed. Intensity peaks falling between predefined minimum and maximum widths and satisfying a minimum prominence were obtained. The obtained peak points were further screened for continuity to identify the axon. The profile of the axon (now in x-y coordinate) was then translated such that the point closest to the CNS was at the origin. The profile was subsequently fitted to a quadratic function. The parameters A and B in Eq. 9 could then be obtained and were used to calculate the average tension and the path length of the axon.

Results

Stiffness and rest tension of axon

The ability to calculate tension using the profile of the axon enabled us to perform a loading experiment by increasing the flow rate. Therefore, we held the flow rate at 0, 20, 40, 60, 100, 140, and 200 μL/min respectively for approximately 3 minutes at each step (Fig. S2 & Movie 1). The immediate elastic response as captured by the dotted line in Fig. S2 were used to calculate axonal stretch (path length difference) and the change in average tension. A tension vs. stretch plot could then be obtained by adding the elastic response sequentially. This procedure allows us to look at the pure elastic response of the axon with minimal influence from the viscous response.

The tension-stretch plot conforms to a linear function with the slope being the stiffness and the y-intercept being the rest tension (Fig. 3a). Since stiffness is length dependent—a longer axon under the same load will lead to a larger deflection, we plotted the stiffness value for each axon tested with respect to their initial length before stretch (Fig. 3b). A 1/length scaling was observed as expected. Note that the length reported here is the exposed length, which was dependent on the sample preparation procedure. The actual length of the axon should be similar in all samples, because their age was controlled. Further comparing to existing literature we found that PC12 axons of 100 - 200 μm in length had stiffness values of 0.4 - 0.5 nN/μm[8,10,14],

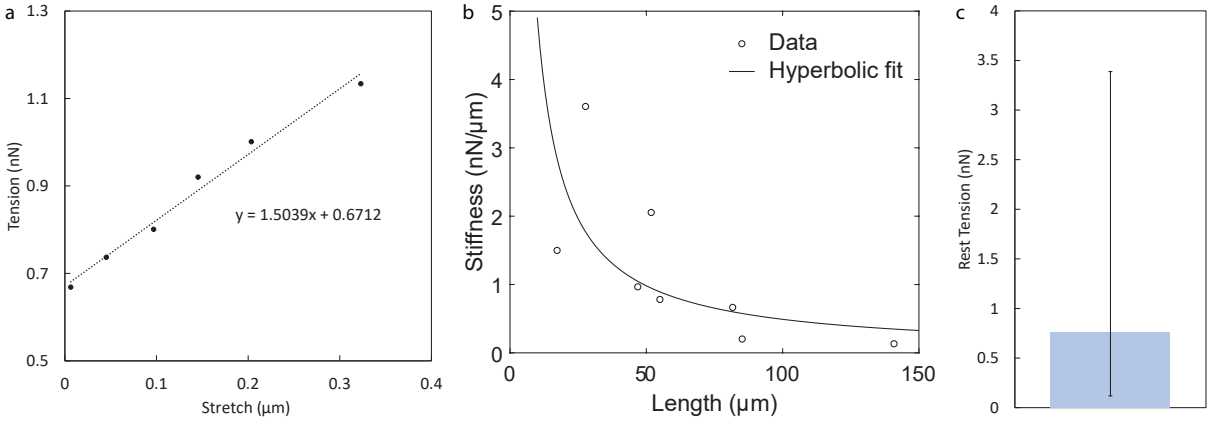

Figure 3: Stiffness and rest tension measurements. (a) An example tension-stretch curve of an untreated axon. By definition, the slope and y-intercept of the linear fit gives the stiffness and rest tension of the axon respectively. (b) Stiffness values of 8 tested axons are reported here. We assess the length (L) dependency of stiffness (K) by fitting $K = \frac{C}{L}$ to the data, as indicated by the black curve. (c) Rest tension values of 8 axons are summarized here. Error bars showing the minimum and maximum tension values.

matching our results in Fig. 3b. We also observed a rest tension range of 0.1 to 3.5 nN (Fig. 3c), agreeing with those reported previously both for *in vitro*[8,10] and *in vivo*[9].

Partial F-actin and myosin disruption can lead to total tension loss without changing an axon's elasticity

After confirming the validity of our setup by comparing our tension and stiffness measurements to that found in the literature, we can then use our setup to partially treat the axons with appropriate drugs. A flow containing cytochalasin D or Y-27632 were applied through one of the center channels (Fig. 4). At the same time, the side channels applied the appropriate saline flow rate such that the central flow can be focused onto only a portion of the axon ($\sim$30 μm[21]). To achieve partial treatment at all times, the total flow rate had to be kept high. Therefore, we held the flow rate at 100 μL/min for 10 minutes. Then the axon was loaded twice more at 140 and 200 μL/min. After the loading paradigm, the flow rate was brought back to 100 μL/min and held for another 10 minutes. However, the central flow was switched off in this case. This way, we intended to wash out the effect of the chemical treatment. The axon was again loaded at 140 and 200 μL/min after the washout. We then repeated the same procedure as described in the previous section to obtain the tension-stretch plots that allowed us to calculate stiffness and rest tension.

Both F-actin and myosin disruptions led to a decrease in rest tension to a negative value, while stiffness remained largely unchanged (Fig, 5a & b). A negative rest tension simply means that the axon would be slack under the unforced condition. We checked this by unloading the axon in a few cases immediately after the partial treatment. The axons did remain slack (Movie 2). This observation is similar to that observed previously in another study[16] where axons were buckled under the influence of acto-myosin disruption. Those axons would remain buckled since contractility was hampered.

To further test the hypothesis of an in series actin-myosin connection, we performed another set of experiments this time shifting the center drug flow (by manipulating the flow ratios) toward the CNS or NMJ side of the axons respectively (Fig. S3a & c). We observed a total loss of tension again in both cases (Fig. S3b & d). Thus, it seems that a local force disruption anywhere along the axon can result in total tension loss, strengthening the in series hypothesis. This result might seem to contradict with the recent observation of contraction strain heterogeneity[24]. However, contraction strain heterogeneity could be the result of actomyosin restoring tension when a tension cannot be sustained during contraction and activities

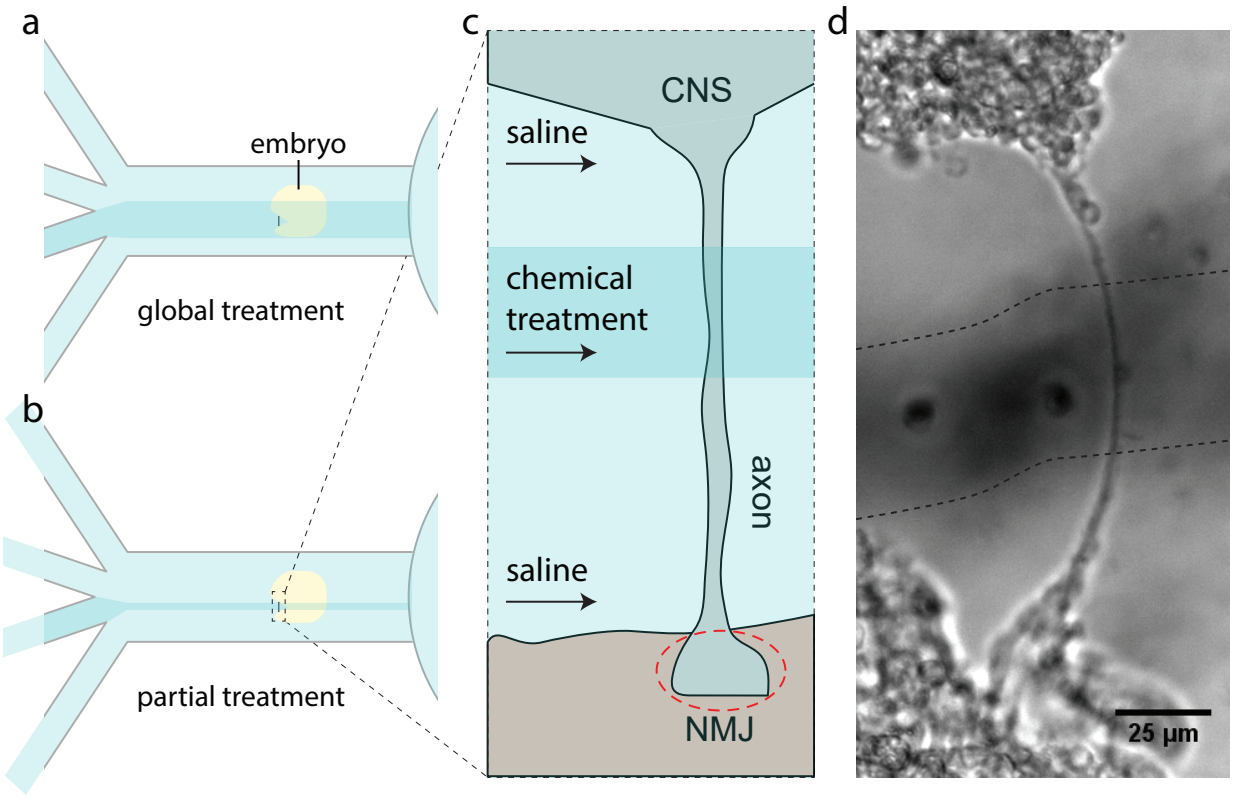

Figure 4: Schematics of (a) global and (b) partial treatments. (c) An expanded schematic of an axon under partial treatment. Only a portion of the axon length is subjected to chemical treatment. (d) An experimental image showing the partial treatment. Contrast created by added food dye.

such as motor slipping. The spatial temporal strain fluctuation demonstrated that actomyosin was active along the entire axon[24].

Partial and global microtubules disruption can lead to axon softening without changing an axon's rest tension

Microtubules are known to provide the structural stiffness for axons[25]. This led us to treat axons with nocodazole to disrupt microtubules both partially and globally to investigate if such would affect the slope in our tension-stretch plots. Indeed, stiffness after washout increased several folds, but rest tension remained the same (Fig. 5c).

We normalized the drug disruptions by dividing the stiffness and tension values for each axon subjected to treatment with the corresponding values after drug washout. This way we compare the same axon with disruption and without disruption. We observed a similar trend that microtubules disruption led to a decrease in stiffness but not rest tension, and acto-myosin disruption led to a decrease in rest tension but not stiffness (Fig. 5d & e). The magnitude of stiffness decrease was more pronounced in global microtubules disruption (Fig. 5d). We therefore inspected the experimental images of axons under partial disruption of microtubules. We found that the curvature within the exposed segment of the axon was significantly higher compared to the segments subjected to saline flow implying low bending rigidity of the microtubule disrupted segment. Since microtubules disruption was localized in the partial treatment cases, the axons retained some of their structural stiffness in the untreated regions (Fig. 5f & g).

Discussion

In this study, we employed a microfluidic setup[21] that can expose a segment of an axon to cytoskeleton disruption drugs to 1) measure the elastic response of the axon, and 2) disrupt F-actin, myosin motors, and microtubules locally at a segment of the axon conduit. This unique approach allowed us to investigate the underlying architecture of the cytoskeletal network.

We revealed that a local F-actin or myosin disruption in axons could lead to a complete intrinsic tension loss without effecting the elastic properties of the axon. We reasoned that this observation could be explained by a connected network of acto-myosin contractile units (Fig. 6). A failure to transmit tension at any point would lead to a total loss of tension in the entire axon.

Local disruption of microtubules, on the other hand, led to a local reduction of bending stiffness, but not the intrinsic tension. This observation agrees with the current view that microtubules plays a passive role in tension generation in axons; they provide resistance to the contractile motion of F-actin and myosin motors, but do not actively generate a force[16].

A recent study provided a functional insight related to our experiments here[21]. Using the same partial treatment system, the study revealed that a local myosin motor disruption away from the synapse can lead to presynaptic vesicle declustering. Using the results of the current study, we reasoned that both global and local disruptions should result in similar magnitude of vesicle declustering due to a total tension loss in the connected tension network. Because of this connectivity in tension transmission, it is possible that a neuron can regulate its synaptic efficacy—which occurs at the distal end—by regulating mechanical tension at the proximal region of its axon or even its cell body.

It was shown that a 20% stretch can lead to the disruption of axonal cytoskeleton structure[17]. Pre-stretch can also lead to an increase in tension. Tension, however, would eventually reduce back to the rest tension level[9]. For these reasons, care was given to minimize pre-stretch during sample preparation. Another concern with sample preparation could be its effect—particularly with the masses just before and after the axon (along the flow direction)—on the flow pattern and hence the applied force. In our experiments, this was unavoidable and hence the exact value of the forces could be difficult to determine. We however

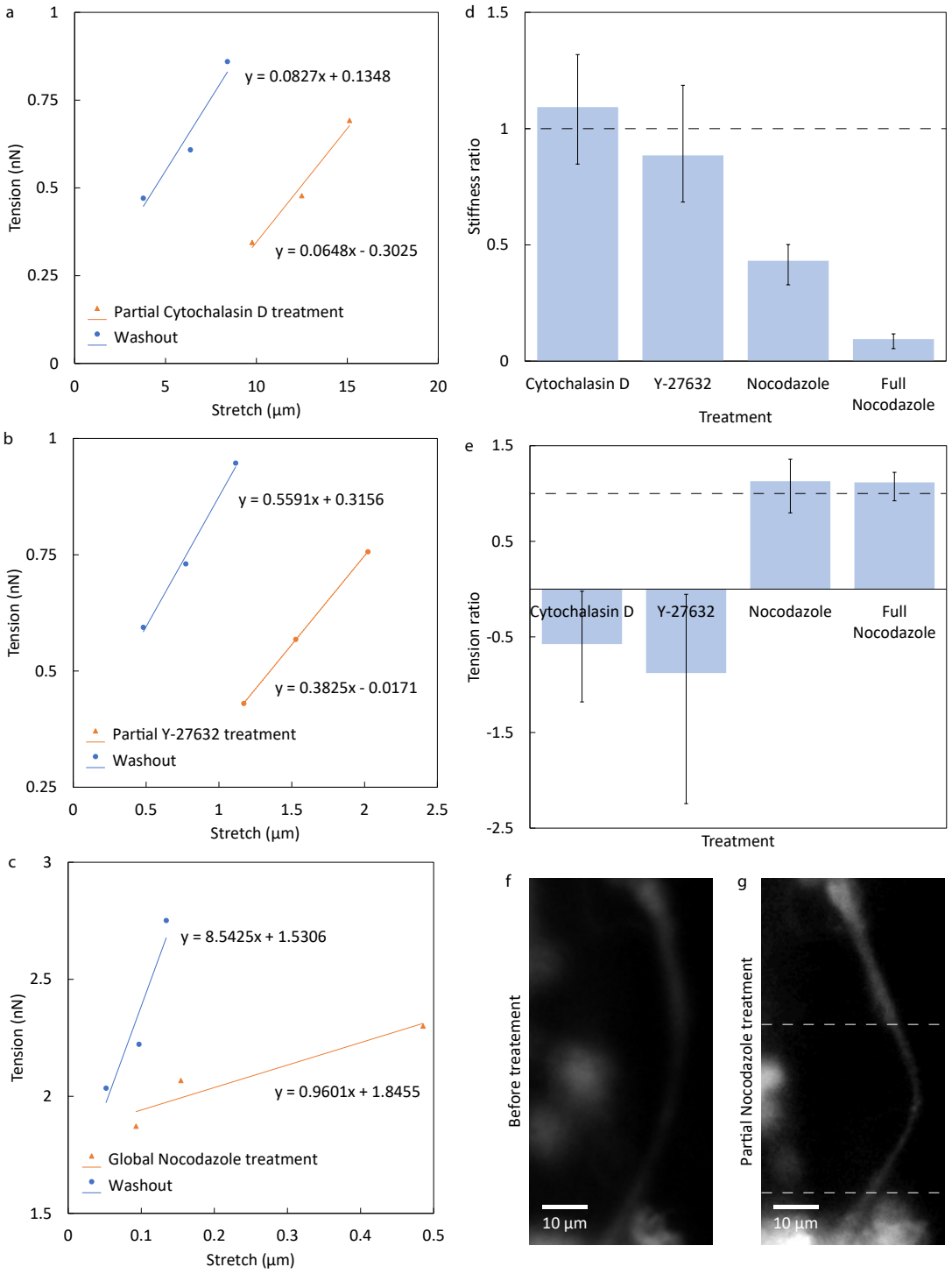

Figure 5: Effects of chemical treatments on axonal stiffness and rest tension. Tension-stretch curves of axons under partial treatment (red) and subsequent PBS washout (blue) using (a) cytochalasin D and (b) Y-27632 to target F-actin and myosin motors respectively. (c) Tension-stretch curves of axons under global treatment (red) and subsequent PBS washout (blue) using nocodazole to target microtubules. (d) Stiffness and (e) tension ratios are obtained by dividing the stiffness and rest tension values under drug disruption with those after washout respectively. The values for all conditions are compared. Dotted lines indicate a ratio of 1 expected for unchanged values. Error bars showing minimum and maximum values. N=3 for all conditions. Results from nocodazole treatment are significantly different than those from Cytochalasin D and Y-27632 treatments ($p < 0.05$). 2-tail student t-test with unequal variance used. An axon (f) before and (g) after partial microtubules disruption is shown. Chemical treatment is applied at the region between the dotted lines, which leads to a more pronounced curvature compared to the other regions.

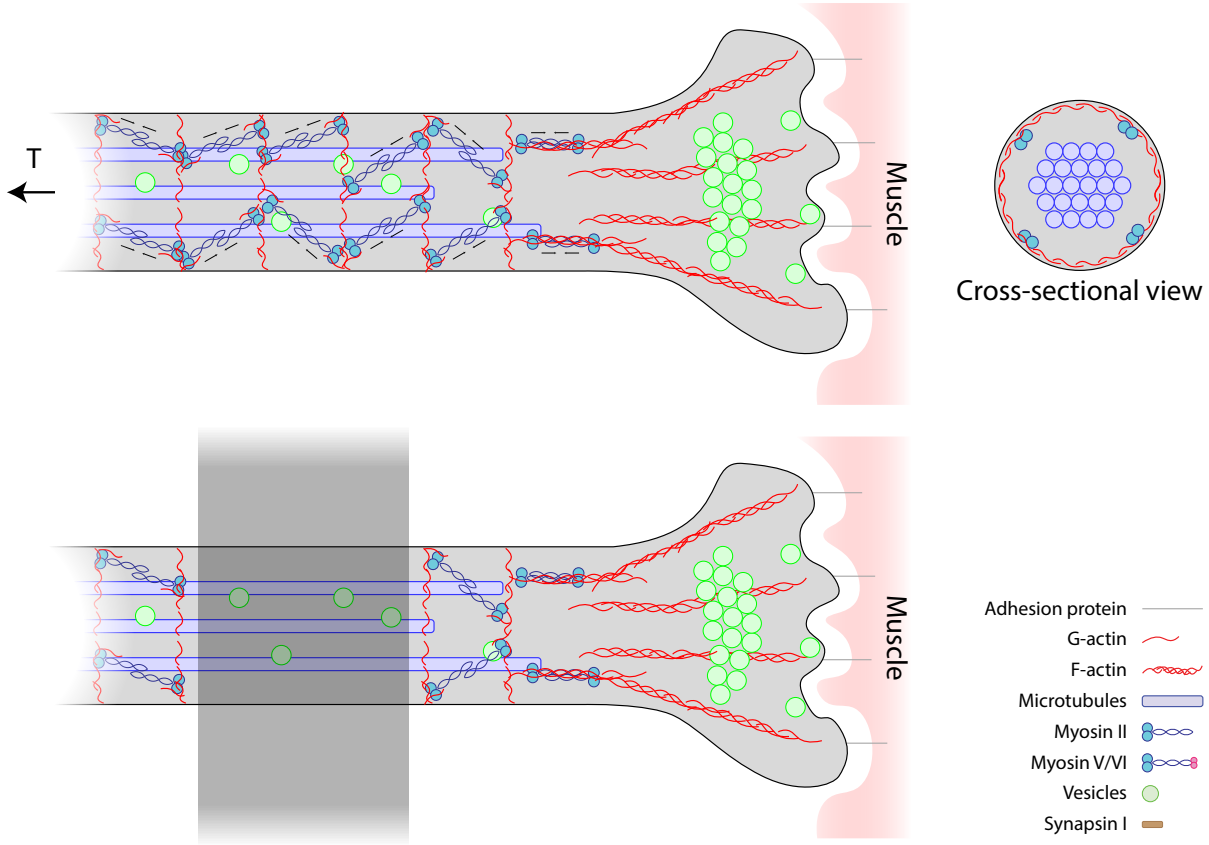

Figure 6: An illustration of the tension generating contractile network. (top) F-actin rings and myosin motors form periodic intercalating units that are actively contractile to generate tension. (bottom) When a disruption occurs locally (black band), the intact units lose the connections in between. Contractile motion might still occur but a tension is not sustained leading to total tension loss.

found that our results in stiffness and rest tension (results derived from the applied flow) matched those reported previously, and thus believe any perturbation to the flow dynamics should not affect the qualitative arguments made.

Another limitation of this study was the width of the drug flow. Ideally, the width should be as narrow as possible such that the drug flow could be used to demonstrate total tension loss at any location. However, further reduction of the width would lead to diffusion mixing resulting in loss of contrast and potency. Caged chemicals could be used for a shorter-term study, but do not combine well with simultaneous force measuring. We believe the exact architecture is best understood using imaging methods; this study aims to provide a paradigm of force generation by the known components within this architecture.

Contribution

AF conceived the study, designed the experiments, conducted the experiments, developed the mechanics model, performed data analysis, and wrote the paper. SJ conducted the experiments. TS supervised the project and wrote the paper.

Conflicts of interest

There are no conflicts of interest to declare.

Acknowledgment

We would also like to thank the Smith-Bolton group at the University of Illinois for fly supplies.

This work was supported by the National Institutes of Health (NINDS NS063405-01), the National Science Foundation (Science and Technology Center on Emergent Behaviors in Integrated Cellular Systems (EBICS) Grant, CBET-0939511, CMMI-1300808, DGE-1144245, and DGE-0965918), and the Croucher Foundation.

References

[1] S. Siechen, S. Yang, A. Chiba and T. Saif, *Proceedings of the National Academy of Sciences of the United States of America*, 2009, **106**, 12611–6.

[2] W. W. Ahmed, T. C. Li, S. S. Rubakhin, A. Chiba, J. V. Sweedler and T. A. Saif, *Cellular and molecular bioengineering*, 2012, **5**, 155–164.

[3] A. Fan, K. A. Stebbings, D. A. Llano and T. Saif, *Frontiers in cellular neuroscience*, 2015, **9**, 292.

[4] D. Bray, *Developmental biology*, 1984, **102**, 379–89.

[5] B. J. Pfister, A. Iwata, D. F. Meaney and D. H. Smith, *The Journal of neuroscience : the official journal of the Society for Neuroscience*, 2004, **24**, 7978–83.

[6] A. Z. Shorr, U. M. Sönmez, J. S. Minden and P. R. LeDuc, *Lab on a chip*, 2019, **19**, 1141–1152.

[7] P. Lamoureux, R. E. Buxbaum and S. R. Heidemann, *Nature*, 1989, **340**, 159–62.

[8] R. Bernal, P. A. Pullarkat and F. Melo, *Physical review letters*, 2007, **99**, 018301.

[9] J. Rajagopalan, A. Tofangchi and M. T. A. Saif, *Biophysical journal*, 2010, **99**, 3208–15.

[10] R. Bernal, F. Melo and P. A. Pullarkat, *Biophysical journal*, 2010, **98**, 515–23.

[11] G. Xu, P. V. Bayly and L. A. Taber, *Biomechanics and modeling in mechanobiology*, 2009, **8**, 253–62.

[12] D. C. van Essen, *Nature*, 1997, **385**, 313–8.

[13] G. Xu, A. K. Knutsen, K. Dikranian, C. D. Kroenke, P. V. Bayly and L. A. Taber, *Journal of biomechanical engineering*, 2010, **132**, 071013.

[14] T. J. Dennerll, H. C. Joshi, V. L. Steel, R. E. Buxbaum and S. R. Heidemann, *The Journal of cell biology*, 1988, **107**, 665–74.

[15] F. J. Ahmad, J. Hughey, T. Wittmann, A. Hyman, M. Greaser and P. W. Baas, *Nature cell biology*, 2000, **2**, 276–80.

[16] A. Tofangchi, A. Fan and M. T. A. Saif, *Biophysical journal*, 2016, **111**, 1519–1527.

[17] A. Fan, A. Tofangchi, M. Kandel, G. Popescu and T. Saif, *Scientific reports*, 2017, **7**, 14188.

[18] K. Xu, G. Zhong and X. Zhuang, *Science (New York, N.Y.)*, 2013, **339**, 452–456.

[19] E. D'Este, D. Kamin, F. Göttfert, A. El-Hady and S. W. Hell, *Cell reports*, 2015, **10**, 1246–51.

[20] S. L. Berger, A. Leo-Macias, S. Yuen, L. Khatri, S. Pfennig, Y. Zhang, E. Agullo-Pascual, G. Caillol, M.-S. Zhu, E. Rothenberg, C. V. Melendez-Vasquez, M. Delmar, C. Leterrier and J. L. Salzer, *Neuron*, 2018, **97**, 555–570.e6.

[21] A. Fan, A. Tofangchi, M. de Venecia and T. Saif, *Lab on a chip*, 2018, **18**, 735–742.

[22] V. Budnik, M. Gorczyca and A. Prokop, *International review of neurobiology*, 2006, **75**, 323–65.

[23] L. D. Landau and E. M. Lifshitz, *Fluid Mechanics*, Elsevier, 2013.

[24] S. P. Mutalik, J. Joseph, P. A. Pullarkat and A. Ghose, *Biophysical journal*, 2018, **115**, 713–724.

[25] E. Kandel, J. Schwartz, T. Jessell, S. Siegelbaum and A. J. Hudspeth, *Principles of Neural Science, Fifth Edition*, McGraw Hill Professional, 2012.